Available online at www.sciencedirect.com
ScienceDirect
Materials Science and Engineering C 28 (2008) 519–525
MATERIALS SCIENCE & ENGINEERING C
www.elsevier.com/locate/msec

Kinetics of elimination and distribution in blood and liver of biocompatible ferrofluids based on Fe_3O_4 nanoparticles: An EPR and XRF study

L.F. Gamarra [a,b,*], W.M. Pontuschka [b], E. Amaro Jr [a,c], A.J. Costa-Filho [d], G.E.S. Brito [b], E.D. Vieira [d], S.M. Carneiro [e], D.M. Escriba [b], A.M.F. Falleiros [f], V.L. Salvador [g]

[a] *Instituto de Ensino e Pesquisa, Hospital Israelita Albert Einstein, São Paulo 05651-901, Brazil*
[b] *Instituto de Física, Universidade de São Paulo, São Paulo 05315-970, Brazil*
[c] *Instituto de Radiologia, Faculdade de Medicina, Universidade de São Paulo, São Paulo 05403-001, Brazil*
[d] *Instituto de Física de São Carlos, Universidade de São Paulo, São Carlos 13560-970, Brazil*
[e] *Laboratório de Biologia Celular, Instituto Butantan, São Paulo 05503-900, Brazil*
[f] *Centro de Ciências Biológicas, Universidade Estadual de Londrina 86051-990, Brazil*
[g] *Centro de aplicações e Lasers, IPEN, São Paulo 05508-000, Brazil*

Received 28 November 2006; received in revised form 6 June 2007; accepted 22 June 2007
Available online 29 June 2007

Abstract

In this study, we evaluated the biodistribution and the elimination kinetics of a biocompatible magnetic fluid, Endorem™, based on dextran-coated Fe_3O_4 nanoparticles endovenously injected into Winstar rats. The iron content in blood and liver samples was recorded using electron paramagnetic resonance (EPR) and X-ray fluorescence (XRF) techniques. The EPR line intensity at $g=2.1$ was found to be proportional to the concentration of magnetic nanoparticles and the best temperature for spectra acquisition was 298 K. Both EPR and XRF analysis indicated that the maximum concentration of iron in the liver occurred 95 min after the ferrofluid administration. The half-life of the magnetic nanoparticles (MNP) in the blood was (11.6±0.6) min measured by EPR and (12.6±0.6) min determined by XRF. These results indicate that both EPR and XRF are very useful and appropriate techniques for the study of kinetics of ferrofluid elimination and biodistribution after its administration into the organism.
© 2007 Elsevier B.V. All rights reserved.

Keywords: EPR; XRF; Ferrofluid; Endorem; Biodistribution; Nanoparticle

1. Introduction

A ferrofluid or magnetic fluid is a stable colloidal dispersion of magnetic nanoparticles (MNP). This is because of the delicate balance among the interactions between the nanoparticles. In particular, the interaction between magnetic moments of neighboring nanoparticles gives rise to magnetic forces and the surfactant molecules, attached to their surface [1]. When these ferrofluids are stable in water with neutral pH and salinity with 0.9% of NaCl [2–6], the physiological conditions are satisfied and the ferrofluids are considered biocompatible. This condition is reached when the magnetic particles are covered with a biocompatible molecular layer to prevent against clustering, changes in the original structure, and biodegradation when exposed to the biological systems [7].

The biocompatible ferrofluids based on oxide nanoparticles are of great interest in clinical applications such as drug-targeting [8], hyperthermia [9], embolotherapy [10], and especially for magnetic resonance imaging contrast agents [11,12].

An important step for optimizing the biocompatible ferrofluid application after its synthesis and characterization and before any implementation of a specific biomedical application, preliminary biological tests must be carried out [3,13–15]. Among these biological tests, it is important to study the ferrofluid biodistribution and elimination after administration into the organism. Dextran-coated iron oxide nanoparticles are known to be internalized (taken up) by Kupffer's cells in the liver and by endothelial cells [16].

* Corresponding author. Instituto de Física da USP - Rua do Matão, Travessa R, 187 ALA 1 SAlA 202-A. CEP 05508-090 Cidade Universitaria, São Paulo - Brasil. Tel.: +55 11 30917073; fax: +55 11 38134334.
E-mail address: lgamarra@if.usp.br (L.F. Gamarra).

0928-4931/$ - see front matter © 2007 Elsevier B.V. All rights reserved.
doi:10.1016/j.msec.2007.06.005

They have been successfully used in magnetic resonance imaging (MRI) detection of human focal hepatic lesions [17–19] and hepatic tumors [18,20]. However, the fate, the MRI images, and the kinetics of the ultrasmall superparamagnetic iron oxide (USPIO) nanoparticles intravenously injected may vary from USPIOs of different origins [21].

The scope of the present work is the study of the kinetics of the biodistribution and the elimination of the biocompatible Fe_3O_4 ferrofluid covered with dextran after intravenous administration to Winstar rats. In this study, electron paramagnetic resonance (EPR) and x-ray fluorescence (XRF) techniques were used to determine the iron content found in the liver and the blood samples of rats.

In the EPR technique, iron ions can be detected only when they present the characteristics of paramagnetic behavior. The six-fold degenerate ground state ^6S of the free ion Fe^{3+} has the electronic configuration $3d^5$ with all of their five electron spins coupled ($S=5/2$) and the total angular momentum equal to zero. In the presence of a local electric field the levels are split in three separate Kramers doublets (Stark effect). Since Fe^{3+} is an ion with odd number of unpaired electrons, the degeneracy of the doublets can only be raised by the application of an external magnetic field thus yielding the paramagnetic resonance spectrum. The overall of EPR spectra of the liver and the blood samples have shown the presence of several paramagnetic species such as iron in molecules like hemoglobin and transferrin [22]; Fe^{3+} free ions [23]; copper proteins, and free radicals [24].

On the other hand, XRF technique is a nondestructive method for elementary analyses, either quantitative or qualitative. The elements contained in the sample are excited by a primary source of white radiation, and the emission of the wavelengths characteristic of each element (fluorescent X-rays) are detected by an adequate detector. These wavelengths and their associated energies are measured, and the elements can be identified and quantified, since the fluorescent X-ray intensity is proportional to the concentration of the elements of interest in the sample.

The study of the MNP eliminations and biodistribution kinetics was carried out in Winstar rats after the administration of the ferrofluid during specific periods, with the purpose of the construction of curves to obtain parameters such as the time elapsed to achieve ferrofluid maximum concentration and the accumulation characteristic time of the nanoparticles in the liver, as well as the characteristic time constant of the MNP elimination in terms of their half-life the nanoparticles elimination from the blood circulation. The EPR and XRF studies were performed in parallel and the results were compared.

2. Materials and methods

2.1. Ferrofluid

The biocompatible ferrofluid Endorem (Endorem™ — Guerbert, earlier trade name AMI-25, Laboratoire Guerbert, France) was used in this work as a proof agent to be injected in rats. It consisted of a suspension of 126.500 mg of Fe_3O_4 superparamagnetic nanoparticles contained in 8 ml of water. The nanoparticles of 4.8–5.6 nm size are coated with low-weight dextran (7–9 kDa) [25] of hydrodynamic diameters between 80–150 nm. In addition to water, the solvent composition consisted of 60.800 mg of dextran, 2.714 mg of citric acid, and 490.400 mg of β-D-mannitol ($C_6H_{14}O_6$). The pharmacokinetics, toxicity, and relativity of this superparamagnetic iron oxide particles have been previously described [26–28]. This biocompatible ferrofluid is currently applied as a contrast agent in MRI.

2.2. Experimental procedure using animals

The experimental procedures using rats were carried out in accordance to animal welfare and local ethics committee regulations.

Sixteen 90-day-old, male Winstar rats with average body weight of 420 g were kept in separate cages, under standard conditions of light and temperature, with alimentation and water at will. The rats were transferred to the experimental laboratory 48 h before the administration of the ferrofluid, for acclimatization purpose.

After fasting, during the night period, they were weighed, and were anesthetized with an intramuscular injection of ketamine chloridrate (100 mg/kg body wt) and xilazine chloridrate (100 mg/kg body wt). After 20 min, they had their cervical region tricotomyzed, and through a small incision in the skin, the subcutaneous plane was exposed and debrided until the jugular vein was exposed.

Next, they received in the jugular vein, during approximately 10 min, an injection of 4 mL of the biocompatible ferrofluid, composed of Fe_3O_4 superparamagnetic nanoparticles (Endorem™ — Guebert), diluted in an isotonic glycolyzed solution, to a final concentration of 15 μmol of Fe/kg body wt, i.e. 0.075 mL/kg body wt, equivalent to 1.52×10^{17} particles of iron per animal.

Following each period of 5, 15, 30, 45, 60, 90, and 180, respectively, two animals were killed and blood samples were collected briefly before, whereas the liver samples were collected after killing. The control samples were collected from two rats not injected with the ferrofluid.

The blood and the liver samples were lyophilized in order to be homogenized for the subsequent EPR and XRF analyses. An Edwards lyophilizer, model E3M8-Modulyo, was used operating at the temperature of −50 °C and pressure of 8×10^{-3} torr, working with a vacuum pump. This process was carried out during a period of 27 h, resulting in a humidity free material.

2.3. EPR spectra of iron entities at different temperatures

Due to our interest to determine the localization of the iron oxide nanoparticles in the EPR spectra, prior to the beginning of the study of the elimination and the biodistribution kinetics of the MNP, it was necessary to determine the iron entities present in the liver and the blood samples of the rats after ferrofluid administration. With this purpose, the EPR spectra of the liver and the blood samples were taken at the temperatures of 4, 100, and 298 K, respectively, searching for the best temperature for the iron oxide nanoparticle resonance. The spectra were recorded using a Bruker ELEXSYS E580 homodyne spectrometer operating in the X band (9.4 GHz).

2.4. EPR and XRF calibration curves

The nanoparticle concentration in the liver and in the blood samples were controlled with the aid of the EPR and the XRF techniques. The calibration curves are shown in Fig. 1, where the dashed line was adjusted to XRF points of known Fe concentrations. Analogous procedure was adopted with the EPR intensities resulting in the solid line.

When the calibration curves are applied to the liver and the blood samples, the EPR and the XRF intensities are proportional to the injected and the distributed ferrofluid, added with the contributions coming from intrinsic ferritin nanoparticles and other eventual unknown components contained in the living organism. All of these superfluous contributions were subtracted from the total measured Fe concentration, as compared with the control samples.

2.4.1. EPR calibration

The EPR line intensity was determined from the area under the absorption line (double integral of the resonance at $g=2.1$), which is proportional to the iron particles concentration per mm^3. The control liver and blood samples mixed with the ferrofluid were used to obtain the calibration curve, i.e., the area under the absorption EPR spectrum around $g=2.1$ as a function of the iron particles concentration per mm^3. This calibration curve is shown in Fig. 1 (solid line). The EPR derivate of the absorption spectrum used to calculate the calibration curve, was obtained at room temperature and it is shown in the inset (b) of Fig. 1. The absorption lineshape is typical of a convoluted cubic crystal powder pattern of a ferromagnetic resonance (FMR) of fine-grained precipitates of ferro- or ferrimagnetic single domains [29,30] also seen when iron ion (Fe^{3+} and Fe^{2+}) dimers and/or clusters are precipitated in glasses [31]. From this curve, a positive first-order magnetocrystalline anisotropy constant $K_1=(1.2\pm 0.2)\times 10^5$ erg/cm^3 was determined from the relation $H_a=2K_1/M_S$, taking into account that the nanoparticles are of magnetite. M_s is the maximum saturation magnetization of the crystal, equal to $H_S/(4\pi/3)$ (erg G^{-1} cm^{-3}) and $H_S\approx 2$ kG for magnetite. The nanoparticles were assumed to be monodomains of spherical shape [30]. From the maximum (H_{max}), minimum (H_{min}) wing, and maximum negative slope (H_{ms}) of the EPR spectrum, the effective g-values are $g_{[100]}=(2.28\pm 0.01)$, $g_{[110]}=(2.02\pm 0.02)$, and $g_{[111]}=(1.94\pm 0.01)$, respectively. The H_a-value is obtained from the field separation between the positions of H_{max} and H_{min} wings (equal to (5/3) H_a). From $H_0=H_{max}-(2/3)H_a$ the value of $g_0=(h\nu/(\beta H_0))=(2.12\pm 0.02)$ is obtained, where $\nu=9.428$ GHz, h is Planck's constant ν is the spectrometer frequency, and β is the Bohr magnetron.

2.4.2. XRF calibration

For the XRF study a calibration curve was determined from the XRF data of a commercial Endorem ferrofluid sample, as well as the standards samples 1577b and 1548a of the National Institute of Standards & Technology. The intensity of the XRF peak associated with iron ions (see inset (c) of Fig. 1) was used to build such calibration curve as shown in Fig. 1 (dashed line). The measures of XRF were accomplished using a Shimadzu XDE-990 device.

Since the intensities measured (in arbitrary units) by XRF and EPR techniques are both proportional to the iron oxide

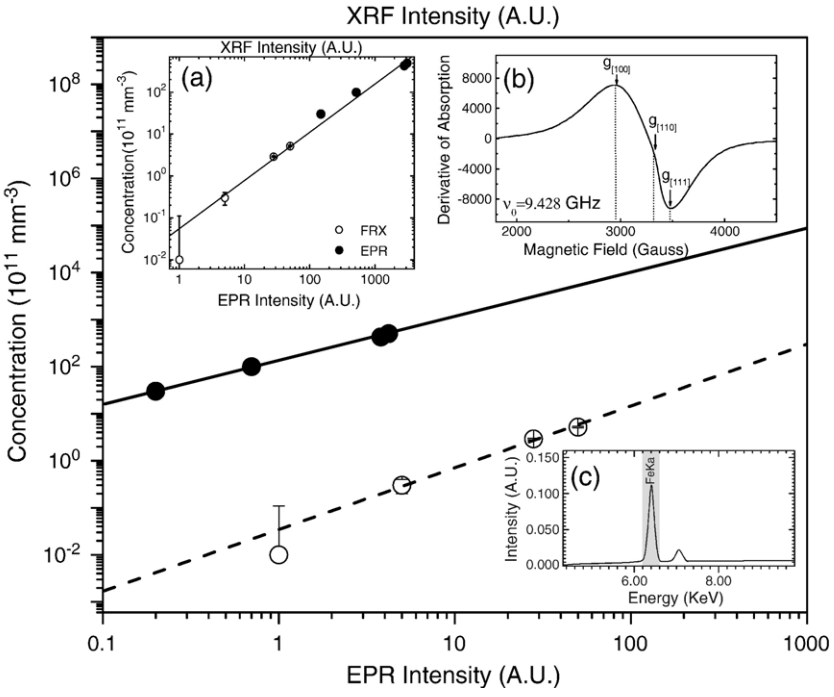

Fig. 1. Calibration curves of EPR (solid line) and XRF (dashed line) of the nanoparticles concentration related with the area under the $g=2.1$ resonance absorption curve and the characteristic FeKa line intensity, respectively. The inset (a) is a single straight line adjusted to the results from both EPR and XRF techniques. The inset (b) is a typical EPR spectrum of the $g=2.1$ line of magnetite contained in the ferrofluid Endorem™ and the inset (c) is the XRF FeKa line, both of them used in the data acquisition for the building of the curve calibration.

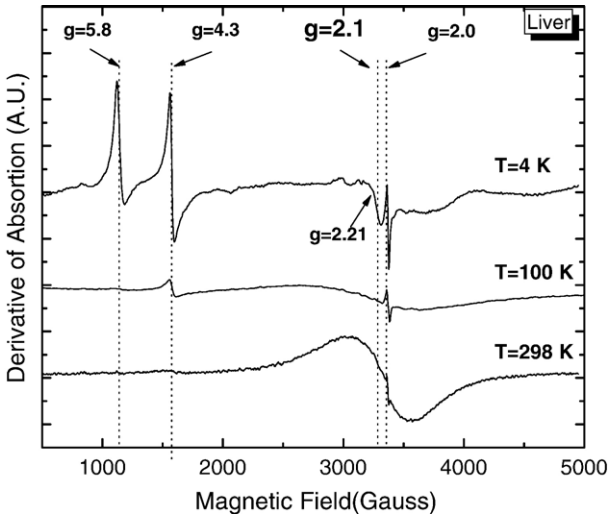

Fig. 2. X-band EPR spectra of the liver at 4, 100 and 298 K. The *g*-values shown in the Fig. are assigned to different iron species present in the sample.

concentrations, it is also possible to unify the results of both techniques in a single calibration curve as shown in the inset (a) of Fig. 1.

3. Results and discussions

3.1. Iron species present in the liver and the blood sample

The iron species in the liver and the blood sample were initially investigated by EPR technique at the temperatures of 4, 100, and 298 K, focusing on the assignment of the resonance's due to the presence of iron in the EPR spectra. The EPR spectra of the liver and the blood samples are shown in Figs. 2 and 3, respectively.

The EPR spectra obtained at the temperatures of 4, 100, and 298 K show the presence of Fe^{3+} ions in hemoglobin ($g=5.8$) that is related to the presence of blood in the whole organism [22]. The signal at $g=4.3$ is typical of transferrin ions Fe^{3+} having rhombic symmetry; this signal may be attributed to the Fe^{3+} ions of the group non-heme of transferrin that is also one of the components of the blood [22]. It was also found that a low-intensity signal at $g=2.21$ attributed to the copper protein, ceruloplasmine, which is a ferroxidase, and whose reduction decreases the iron transport to eritroproteic sites [32]. The resonance at $g=2.0$ is attributed to a free radical, usually found in the tissues [24]. In this work, the resonance at $g=2.1$ is the sum of the contributions from the injected ferrofluid [3,33,34] internalized into the cells of the mononuclear phagocytic system, such as the Kupffer cells in the liver [34] and the Fe^{+3} ions of ferritin grains [22], so that the contributions from the control samples were subtracted, as explained above.

The EPR signals from iron ions of hemoglobin and transferrin are barely detected at room temperature, due to their fast relaxation times, as it is shown in Figs. 2 and 3. However, the intensity of the resonance coming from ferritin, identified as the broad component at $g=2.1$, decreases with the decreasing temperature as observed in Fig. 2 for temperatures of 298 and 100 K and it is observed in Fig. 3 only for $T=298$ K. This behavior of $g=2.1$ resonance with temperature was already reported in the literature [22], in agreement to the suggested formation of an antiferromagnetically ordered phase at 4 K. The EPR spectra of the liver sample at 4 K are very similar to those observed in the same conditions for the blood samples.

The EPR lines attributed to Fe^{2+} ions of hemoglobin ($g=5.8$) and Fe^{3+} ions of transferrin ($g=4.3$) are less prominent at 100 K than those observed at the temperature of 4 K (Figs. 2 and 3). In the same spectrum, the contribution of superparamagnetic nanoparticles ($g=2.1$) is noticed.

The EPR spectra at 298 K (Figs. 2 and 3) show a broad line in the region of $g=2.1$ from the Fe^{3+} ions of ferritin and from the dominant contribution of the superparamagnetic nanoparticles of the ferrofluid [35]. This signal shows a broadening with decreasing temperature, due to an increasing blocking of the magnetization of the superparamagnetic nanoparticles.

In the EPR spectra measured at 298 K, it is basically seen in the broad line at $g=2.1$ and assigned to superparamagnetic particles present in the liver and the blood samples. Since our main interest is to study those particles, we chose 298 K as our working temperature. Confirming in this way the value of temperature chosen for the present study corresponds to those values reported in the literature [3,15,34,36].

The room temperature ($T=298$ K) was selected because the $g=2.1$ resonance increased with the increase of temperature. Further heating will probably introduce eventual irreversible changes probably damaging the samples.

3.2. EPR and XRF study of ferrofluid elimination kinetics in the blood

The study of elimination kinetics of the ferrofluid in the blood was carried out using the EPR technique [15]. The concentration of the nanoparticles was determined from the area under the EPR absorption spectra, which was compared with the values used in the calibration curve (Fig. 1 (solid line)). The EPR spectra were recorded in the periods established by the protocol (see above) and are shown in Fig. 4.

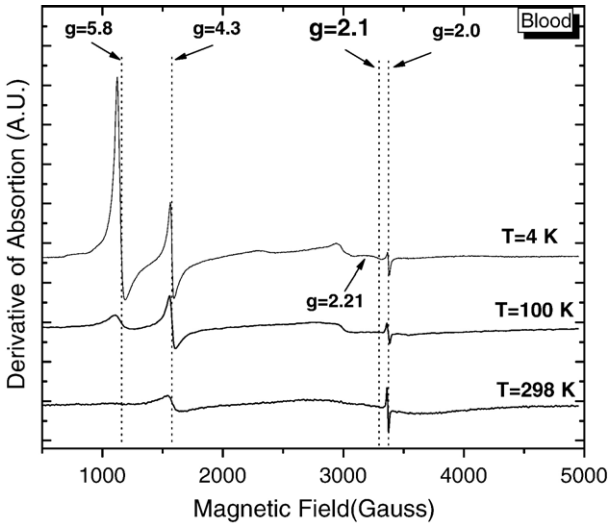

Fig. 3. EPR spectra of blood at 4, 100, and 298 K.

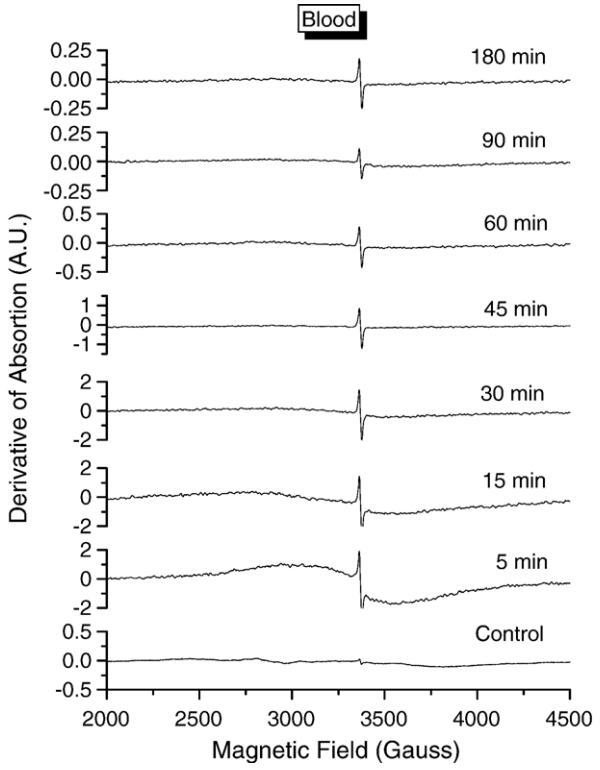

Fig. 4. EPR spectra at room temperature of the lyophilized blood, after ferrofluid administration in the different periods for the study of the elimination kinetics of the ferrofluid.

Fig. 5 (continuous line) reproduces the time decay of the concentration of Fe_3O_4 nanoparticle in the blood sample measured by EPR technique. From this data it is clear that the injected solution is rapidly eliminated from the circulation, and almost the totality of the iron oxide nanoparticles disappear about 60 min after the fluid administration. The continuous line in Fig. 5 represents the adjustment of data using a first-order exponential decay [37]. Thus, the time dependence of the nanoparticle concentration $C(t)$ in the blood sample is given by [3,15,36]:

$$C(t) = C_0^B e^{-\frac{t}{\tau_B}}, \quad (1)$$

where C_0^B is the concentration of nanoparticles at time $t=0$ and τ_B is the characteristic time constant of the nanoparticles elimination from the blood, which is equivalent to the time needed to eliminate 63% of the concentration of the administered nanoparticles.

The fitting of the data in Fig. 5 for the blood sample to Eq. (1) led to the parameter values $C_0^B=(7.3\pm0.1)\times10^{12}$ particles/mm^3 and $\tau_B=(16.8\pm0.8)$ min. The half-life of the nanoparticles elimination process in the blood circulation is given by $t_{1/2}=\tau_B$ Ln2$=(11.6\pm0.6)$ min.

The time decay of the concentration of iron oxide nanoparticles in the blood sample as measured by XRF technique is also shown in Fig. 5 (open symbols and dashed line). The nanoparticle concentrations were determined from the characteristic FeKa line from the samples and interpolating with the

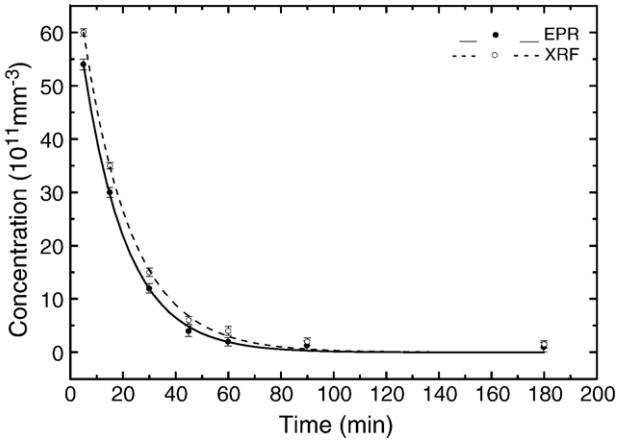

Fig. 5. Ferrofluid elimination kinetic curves constructed from the EPR (●) and XRF (○) spectra of blood samples.

calibration curve of Fig. 1 (dashed line). Fitting of data to Eq. (1) yielded the parameters $C_0^B=(7.8\pm0.2)\times10^{12}$ particles/mm^3 and $\tau_B=(18.2\pm0.8)$ min. The half-life associated with the nanoparticles behavior is $t_{1/2}=(12.6\pm0.6)$ min.

3.3. EPR and XRF study of ferrofluid biodistribution kinetics in the liver

The EPR study of the ferrofluid biodistribution kinetics in the liver was carried out in a similar way as for the blood sample. The concentration of the nanoparticles was determined from the area under the resonance absorption curves of the EPR spectra during

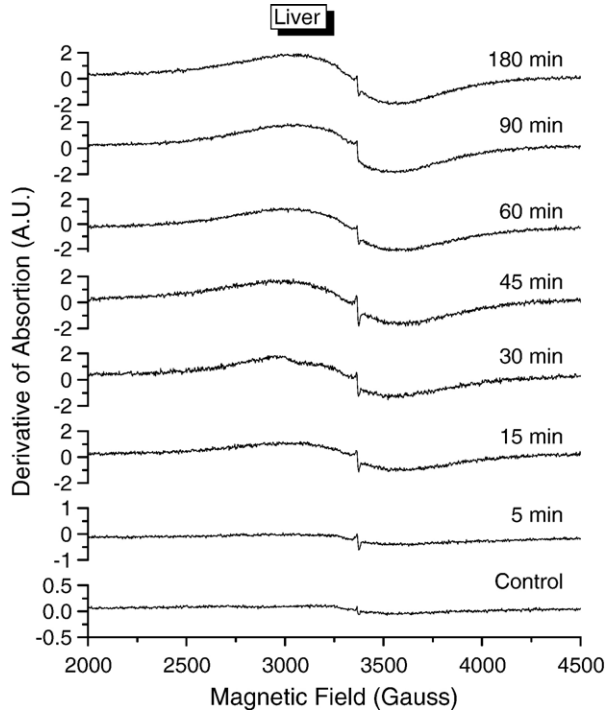

Fig. 6. EPR spectra at room temperature of the lyophilized liver, after the ferrofluid administration in different periods, for the study of the ferrofluid biodistribution kinetics.

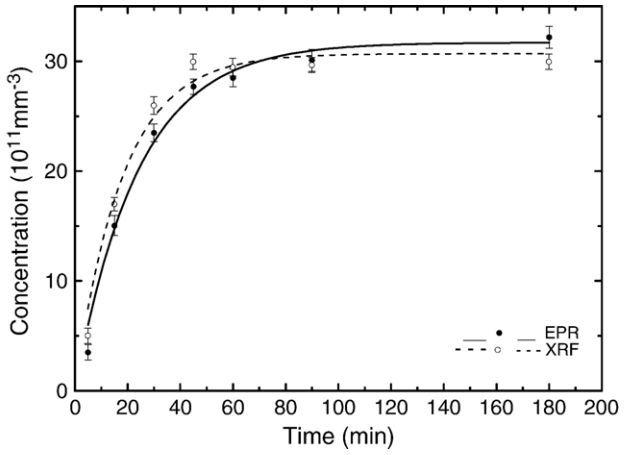

Fig. 7. Curves of the ferrofluid biodistribution kinetics constructed from the EPR (●) spectra and the XRF (○) characteristic lines of iron for the liver samples.

the periods established in the protocol (see Fig. 6) and subsequent comparison with the values in the calibration curve (Fig. 1(solid line)).

The curves of Fig. 7, obtained from the EPR spectra (continuous line) and the XRF (dashed line) suggest that the magnetic nanoparticles are transferred from the blood current system to the liver. It is known, however, that the MNP of iron oxide are not transferred only to the liver, but they are also distributed to several other organs of the rat [38].

The time dependence of the nanoparticles concentration $C(t)$ is given by [3,15,36]:

$$C(t) = C_0^{\mathrm{L}}\left[1 - e^{-\frac{t}{\tau_{\mathrm{L}}}}\right], \qquad (2)$$

where C_0^{L} is the maximum concentration of nanoparticles accumulated in the liver, and τ_{L} is the characteristic time constant of the nanoparticles accumulation in the liver, which is equivalent to the time necessary for accumulating 63% of the maximum concentration.

From the fitting of the EPR data in Fig. 7 to Eq. (2), we obtained $C_0^{\mathrm{L}}=(32\pm1)\times10^{11}$ particles/mm^3 and $\tau_{\mathrm{L}}=(24\pm2)$ min.

For the ferrofluid biodistribution kinetics in the liver, the nanoparticles concentrations measured by XRF were obtained by the same procedure adopted with the blood samples. From the adjustment of the data of Fig. 7, using Eq. (2), it was determined $C_0^{\mathrm{L}}=(31\pm1)\times10^{11}$ particles/mm^3 and $\tau_{\mathrm{L}}=(19\pm2)$ min.

4. Conclusion

The iron entities present in the liver and the blood samples of rats were quantified using the EPR resonance of interest at $g=2.1$. It was observed that the best condition to observe this resonance occurs at room temperature.

From the EPR study it was observed a decay kinetic of first order in the MNP concentration in the blood circulation, with half-time of (11.6±0.6) min and the characteristic time constant of the nanoparticles elimination of (16.8±0.8) min. These values are in excellent agreement with those parameters obtained from the XRF measurements, which yielded (12.6±0.6) min for the half-life, and the characteristic time constant of the nanoparticles elimination of (18.2±0.8) min.

The EPR study of the biodistribution in the liver has led to the results of $(32\pm1)\times10^{11}$ particles/mm^3, with a characteristic time constant of nanoparticles accumulation of (24±2) min. These parameters were also found through the technique of XRF with $(31\pm1)\times10^{11}$ particles/mm^3 as maximum reached concentration and characteristic time constant of nanoparticles accumulation of (19±2) min. The agreement between these results makes evident that both EPR and XRF are very appropriate techniques for the study of elimination and biodistribution kinetics of the MNP of Fe_3O_4 coated with dextran and administered to rats.

Acknowledgments

The authors are grateful to CAPES, CNPq, IIEP-Hospital Israelita Albert Einstein and Instituto do Milênio de Fluidos Complexos for the financial support of this work.

References

[1] R.P. Pant, Rashmi, R.M. Krishna, P.S. Negi, K. Ravat, U. Dhawan, S.K. Gupta, D.K. Suri, J. Magn. Magn. Mater. 149 (1995) 10.
[2] P.C. Moraes, R.L. Santos, A.C.M. Pimenta, R.B. Azevedo, E.C.D. Lima, Thin solid Films 515 (2006) 266.
[3] L.M. Lacava, Z.G.M. Lacava, M.F. da Silva, O. Silva, S.B. Chaves, R.B. Azevedo, F. Pelegrini, C. Gansau, N. Buske, D. Sabolovic, P.C. Morais, Biophys. J. 80 (2001) 2483.
[4] A.C. Tedesco, D.M. Oliveira, Z.G.M. Lacava, R.B. Azevedo, E.C.D. Lima, P.C. Moraes, J. Magn. Magn. Mater. 272–276 (2004) 2404.
[5] Cecilia Albornoz, Silvia E. Jacobo, J. Magn. Magn. Mater. 305 (2006) 12.
[6] R. Langer, Science 249 (1990) 1527.
[7] P. Tartaj, M. del Puerto, S. Morales, F. Veintemillas-Verdaguer, T. González-Carreño, C. Serna, J. Phys., D. Appl. Phys. 36 (2003) R182.
[8] A.S. Lübbe, C. Bergemann, W. Huhnt, T. Fricke, H. Reiss, J.W. Brock, D. Huhn, Cancer Res. 56 (1996) 4694.
[9] A. Jordan, R. Scholz, P. Wust, H. Fähling, R. Felix, J. Magn. Magn. Mater. 201 (1999) 413.
[10] J. Liu, G.A. Flores, R. Sheng, J. Magn. Magn. Mater. 225 (2001) 209.
[11] L. Babes, B. Denizot, G. Tanguy, J.J.L. Jeune, P. Jallet, J. Colloid Interface Sci. 212 (1999) 474.
[12] D.K. Kim, Y. Zhang, J. Kehr, T. Klason, B. Bjelke, M. Muhammed, J. Magn. Magn. Mater. 225 (2001) 256.
[13] Z.G.M. Lacava, R.B. Azevedo, L.M. Lacava, E.V. Martins, V.A.P. Garcia, C.A. Rebola, A.P.C. Lemos, M.H. Sousa, F.A. Tourinho, P.C. Morais, M.F. da Silva, J. Magn. Magn. Mater. 194 (1999) 90.
[14] Z.G.M. Lacava, E.V. Martins, M.L.L. Freitas, E.M.S. Coelho, M.H. Sousa, M.F. da Silva, R.B. Azevedo, F.A. Tourinho, P.C. Morais, J. Magn. Magn. Mater. 201 (1999) 431.
[15] L.M. Lacava, Z.G.M. Lacava, R.B. Azevedo, S.B. Chaves, V.A.P. Garcia, O. Silva, F. Pelegrini, N. Buske, C. Gansau, M.F. da Silva, P.C. Morais, J. Magn. Magn. Mater. 252 (2002) 367.
[16] P.F. Hahn, D.D. Stark, R. Weissleder, G. Elizondo, S. Saini, J.T. Ferruci, Radiology 174 (1990) 361.
[17] P. Reimer, R. Weissleder, A.S. Lee, S. Buettner, J. Wittenberg, T.J. Brady, Radiology 178 (1991) 769.
[18] E.R. Wisner, E.G. Amparo, D.R. Vera, J.M. Brock, T.W. Barlow, S.M. Griffey, C. Drake, R.W. Katzberg, JCAT 19 (1995) 211.
[19] S.H. Duda, M. Laniadio, A.F. Kopp, E. Gronewaller, K.P. Aicher, P. Pavone, E. Jehle, C.D. Claussen, J. Magn. Reson. Imaging 4 (3) (1994) 309.

[20] P. Reimer, R. Weissleder, A.S. Lee, J. Wittenberg, T.J. Brady, Radiology 177 (1990) 729.
[21] B. Dupas, M. Berreur, R. Rohanizadeh, B. Bonnemain, K. Meflah, G. Pradal, Biol. Cell 91 (1999) 195.
[22] A. Slawska-Waniewska, E. Mosiniewicz-Szablewska, N. Nedelko, J. Galazka-Friedman, A. Friedman, J. Magn. Magn. Mater. 272–276 (2004) 2417.
[23] E. Linares, L.S. Nakao, A. Ohara, M.B. Kadiiska, Free Radic. Biol. Med. 34 (2003) 766.
[24] L. Zecca, T. Shima, A. Stroppolo, C. Goj, G.A. Battiston, R. Gerbasi, T. Sarna, H.M. Swartz, Neuroscience 73 (1996) 407.
[25] M. Laniado, A. Chachuat, Verträglichkeitsprofil von ENDOREM, Radiologe, vol. 35, 1995, p. S266, (Suppl. e).
[26] J.T. Halavaara, A.E. Lamminen, S. Bondestam, C.G. Standertskjoeld-Nordenstam, L.M. Hamberg, JCAT 18 (1994) 897.
[27] R. Weissleder, B.L. Engelstad, B.R. Bacon, D.L. White, P. Jacobs, J. Lewis, AJR 152 (1989) 167.
[28] S. Majumdar, S.S. Zoghbi, J.C. Gore, Invest. Radiol. 25 (1990) 771.
[29] D.L. Griscom, J. Non-Cryst. Solids 67 (1984) 81.
[30] C.S. Ray, S.T. Reis, W.M. Pontuschka, J.B. Yang, F.F. Sene, J.M. Giehl, C.W. kim, S. Sen, J. Non-Cryst. Solids 352 (2006) 3677.
[31] S.T. Reis, D.L.A. Faria, J.R. Martinelli, W.M. Pontuschka, D.E. Day, C.S.M. Partiti, J. Non-Cryst. Solids 304 (2002) 189.
[32] V.V. Rylkov, M.Y. Tarasiev, K.A. Moshkov, Eur. J. Biochem. 197 (1991) 185.
[33] V.K. Sharma, F. Waldner, J. Appl. Phys. 48 (1977) 4298.
[34] L.M. Lacava, V.A.P. Garcia, S. Kückelhaus, R.B. Azevedo, Z.G.M. Laçava, O. Silva, F. Pelegrini, C. Gansau, N. Buske, P.C. Morais, J. Appl. Phys. 93 (2003) 7563.
[35] K. Nagata, A. Ishihara, J. Magn. Magn. Mater. 104–107 (1992) 1571.
[36] N. Sadeghiani, L.S. Barbosa, M.H.A. Guedes, S.B. Chaves, J.G. Santos, O. Silva, F. Pelegrini, R.B. Azevedo, P.C. Moraes, Z.G.M. Laçava, IEEE Trans. Magn. 41 (10) (2005) 4108.
[37] P. Nony, M. Cucherat, J.P. Boissel, Trends Pharmacol. Sci. 19 (1998) 49.
[38] R. Weissleder, A. Bogdanov, E.A. Neuweltb, M. Papisov, Adv. Drug. Deliv. Rev. 16 (1995) 321.